MISO Regulates Mitochondria Dynamics and mtDNA Homeostasis by Establishing Inner Membrane Subdomains

Yue Zhang[1], Yuchen Xia[1], Xinhui Wang[1], Shang Wu[1], Jianshuang Li[2], Xuan Guo[3*], Qinghua Zhou[2*], Li He[1,*]

1. The First Affiliated Hospital of USTC, Division of Life Sciences and Medicine, University of Science and Technology of China, Hefei, 230027, China

2. The Biomedical Translational Research Institute, Health Science Center (School of Medicine), Jinan University, Guangzhou, Guangdong, 510632, China

3. Life Science Institute, Jinzhou Medical University, Jinzhou, Liaoning, 121001, China

*For Correspondence:

lihe19@ustc.edu.cn

gene@email.jnu.edu.cn

guoxuan@jzmu.edu.cn

Abstract

Mitochondrial dynamics and mtDNA homeostasis are critical in various biological processes, including cell fate determination, metabolism, and aging. Although specialized mitochondrial membrane subdomains linking these two aspects have recently been reported, their structural and molecular characteristics have remained elusive. In this study, we discover MISO (**M**itochondrial **I**nner membrane **S**ubdomain **O**rganizer), a novel protein that initiates the formation of distinct **M**ISO-**E**nriched **M**itochondrial **S**ubdomains (MEMS) within the inner mitochondrial membrane. Our data demonstrate that MISO is an evolutionary conserved protein that regulates mitochondrial dynamics in *Drosophila* intestinal stem cells (ISCs) *in vivo* and various human and mouse cell lines *in vitro*. The functions of MISO depend on the formation of MEMS, which promote mitochondrial fission while inhibiting fusion, likely through the modulation of FIS1-DRP1 and OPA1 respectively. Further investigation reveals that MEMS recruit mtDNA nucleoids, facilitating their degradation via peripheral mitochondrial division. Additionally, we show that MISO orchestrates the assembly of MEMS through oligomerization mediated by its C-terminal domain, which drives contact between

inner mitochondrial membranes to generate locally multilayered structures. Our findings collectively elucidate the molecular identity and functional mechanisms of specific mitochondrial subdomains both *in vivo* and *in vitro*, revealing a structural link between the regulation of mitochondrial dynamics and mtDNA homeostasis.

Introduction

Mitochondria, as the primary metabolic and signaling centers within eukaryotic cells, play critical roles in a myriad of essential cellular processes. Over 40% of mitochondrial proteins have been linked to human diseases, highlighting their significance in human pathology. A recent major advancement in mitochondrial biology has been the recognition of spatial heterogeneity within the mitochondrial network, revealing that distinct regions of mitochondria can exhibit specialized functions. Among the most well-studied subdomains are the contact sites between the endoplasmic reticulum (ER) and mitochondria. These ER-mitochondria junctions modulate lipid exchange, calcium signaling, mitochondrial division, and the replication of mitochondrial DNA (mtDNA) [1]. Other specialized membrane regions, defined by contacts between mitochondria and lysosomes, the Golgi apparatus, and lipid droplets, have also been shown to regulate mitochondrial dynamics and metabolic status [2-4]. A subpopulation of mitochondria has been discovered to be specialized for the production of proline and ornithine [5]. Additionally, aged or nutrient-stressed yeasts generate specialized compartment for protein degradation called mitochondrial-derived compartment (MDC) [6, 7], while infection of mammalian cells by *Toxoplasma gondii* leads to the formation of distinct structures positive for the outer mitochondrial membrane, termed SPOTs [8]. Despite these advancements, our knowledge regarding the existence and functionality of different mitochondrial subdomains remains limited. Whether additional functional subdomains, organized by specific molecular regulators, exist within mitochondria continues to be an open and compelling question in the field.

A recent live-imaging study has uncovered a unique mitochondrial behavior termed peripheral fission. This process, specifically regulated by the mitochondrial fission protein 1 (FIS1), enables the segregation of damaged mitochondrial components into smaller fragments for

targeted degradation [9]. Subsequent research revealed that the mitochondrial fission process 1 (MTFP1) protein facilitates the partitioning of mtDNA into small MTFP1-enriched mitochondria (SMEM) through this peripheral fission mechanism [10]. However, the absence of MTFP1 does not prevent the formation of specialized mitochondrial subdomains characterized by the enrichment of prohibitin 2 (PHB2) [10] , suggesting that the core regulator of peripheral fission remains unidentified.

In this study, using both *Drosophila* and mammalian cells as model systems, we addressed this gap by providing molecular and structural insights into the linkage between mitochondrial dynamics and mtDNA maintenance. Specifically, we identified an evolutionary conserved protein and functional mitochondrial subdomain that elucidates the molecular mechanism underlying peripheral mitochondrial fission. Our study demonstrated the role of a key protein in orchestrating the formation of this specialized membrane structure, thereby establishing a direct link between the regulation of mitochondrial dynamics and the maintenance of mtDNA homeostasis.

Results

Identification of CG30159/MISO as a novel mitochondria protein that forms inner membrane subdomains and promotes mitochondria fission in *Drosophila* intestinal stem cells.

In a previous genetic screen aimed at identifying genes enriched in *Drosophila* intestinal stem cells (ISCs), we uncovered the *CG30159* gene. Both loss-of-function and gain-of-function of this gene significantly affected ISC proliferation [11]. Bioinformatic analysis predicts that *CG30159* encodes a putative secreted protein, given the presence of a signal peptide-like sequence at its N-terminus. Despite this prediction, the precise molecular function of CG30159 remains elusive. Its human homologue, C3orf33, has been identified in a genetic screen as a suppressor of ERK signaling; however, the mechanisms underlying this inhibitory effect are still unclear [12].

To elucidate the biological function of *CG30159*, we first inserted a *Gal4* gene downstream of

the start codon (ATG) of *CG30159*. This integration allows the expression pattern of *Gal4* to faithfully reflect that of *CG30159*, thereby facilitating the identification of tissues and cells where *CG30159* is expressed (**Fig. 1a**). Subsequent analysis demonstrated that *CG30159* is prominently expressed in *esg+* stem cells of the fly midgut, including both ISCs (identified by *Delta* staining) and enteroblasts (identified by *Su(H)Gbe-LacZ* staining) (**Figure 1b, Supplementary Fig. 1a-d**). Next, we introduced a C-terminal HA-tagged CG30159 (CG30159-HA) into ISCs to investigate its subcellular localization, and found that CG30159-HA protein formed multiple punctate structures resembling intracellular vesicles (**Fig. 1c**). To determine the precise subcellular localization of CG30159, we performed immuno-electron microscopy on fly midgut expressing CG30159-HA in ISCs, using gold particle-conjugated antibodies against the HA tag. Strikingly, all nano-gold particles were found within the mitochondria, indicating that CG30159 is a mitochondrial protein (**Fig. 1d**). This finding is corroborated by two independent proteomic studies employing APEX proximity-labeling in *Drosophila* and mammalian cells, which identified CG30159 and its human ortholog C3orf33 as proteins residing within the mitochondrial matrix or inner membrane[13, 14].

Considering that mitochondria in ISCs typically exhibit filamentous structures, it raises questions regarding the punctate appearance of CG30159. To investigate this phenomenon, we co-labeled CG30159 and mitochondria in ISCs for observation. To our great surprise, the CG30159 puncta were found to be "bud-like" membrane subdomains encircling the tips of mitochondria (**Fig. 1e**). This specific localization of CG30159 to mitochondrial subdomains was further validated in cultured *Drosophila* S2 cells, where a different tag (3×Flag) was introduced at the N-terminus of CG30159, suggesting that the observed localization is not an artifact of the tag fusion (**Supplementary Fig. 1e**). Given that some proteins may form unnatural aggregates when overexpressed, we further generated a knock-in allele with a 3×HA tag at the C-terminus of endogenous CG30159 (**Fig. 1f**). Our data showed that the CG30159-HA[KI] protein is enriched in the midgut stem cells of flies (**Fig. 1g**) and also forms numerous subdomains on mitochondria, even when expressed at physiological levels (**Fig. 1h**). These endogenously tagged subdomains are similar in location to those induced by overexpression, albeit smaller in size, suggesting that CG30159 naturally accumulates in specific regions of the

mitochondrial membrane.

Given that CG30159 is a mitochondrial protein, we further studied the impact of altering CG30159 levels on mitochondrial morphology in ISCs. Knocking down CG30159 in ISCs resulted in an elongated mitochondrial phenotype (**Fig. 1i-j**), whereas prolonged overexpression of CG30159 led to pronounced mitochondrial fragmentation (**Fig. 1k-l**). These observations suggest that CG30159 functions as novel regulator of mitochondrial morphology. These observations demonstrate that CG30159 is likely to be a novel regulator of mitochondrial morphology.

Since the expression of CG30159 significantly enhances the formation of the mitochondrial subdomains, which can be visualized through the mitochondrial matrix-localized mito-APEX--Flag (**Fig.1k-l**), we decided to rename this gene as **M**itochondrial **I**nner membrane **S**ubdomain **O**rganizer (MISO), and refer to this protein as MISO in all subsequent studies.

The ability of MISO to form mitochondrial subdomains and regulate mitochondrial morphology is evolutionarily conserved in mammals.

MISO is an evolutionary conserved protein across major metazoan species, from sea sponge to human (**Fig. 2a**). The MISO protein typically comprises a short N-terminus of approximately 40 amino acids, a transmembrane domain of around 22 amino acids (previously considered to be a signal peptide for secretion), a highly conserved core domain predicted to fold into a beta-barrel structure, and a less conserved region at the a less conserved region that is expected to form 3-4 alpha helices (**Fig. 2a, Supplementary Fig. 2a**). In human, two isoforms of MISO/C3orf33 have been identified, with the shorter isoform lacks the first 43 amino acids at the N-terminus.

To investigate the biological function of MISO, we generated human osteosarcoma U2OS cells with both MISO isoforms knocked out (MISO-KO) using CRISPR-Cas9. Similar to observations in fly intestinal stem cells (ISCs), mitochondria in MISO-KO cells displayed a pronounced hyper-fusion phenotype (**Fig. 2b-d**). Additionally, knocking down MISO using two

independent shRNAs targeting both isoforms resulted in comparable mitochondrial fusion phenotypes in U2OS cells, as well as in human hepatoma PLC/PRF/5 and Huh7 cells (**Supplementary Fig. 2b-h**), suggesting that MISO performs similar functions across different human cell types. Furthermore, we generated a MISO-KO mouse strain using CRISPR-Cas9 (**Supplementary Fig. 2i**). These MISO-KO mice exhibited no significant developmental or reproductive defects. However, primary hepatocytes and mouse embryonic fibroblasts (MEFs) isolated from MISO-KO mice showed a significant hyper-fused mitochondrial phenotype compared to those from wild-type (WT) mice (**Supplementary Fig. 2j-m**). Meanwhile mitochondrial stress generated by carbonyl cyanide m-chlorophenyl hydrazone (CCCP) treatment triggered similar degree of mitochondrial fragmentation in MISO-WT and MISO-KO U2OS cells, suggesting that MISO is not an indispensable component of mitochondria fission (**Supplementary Fig. 2n-o**). This modulatory role of MISO may be attributed to its relatively late evolutionary appearance in multicellular organisms. Collectively, our data suggests that MISO plays an evolutionarily conserved role in regulating mitochondrial dynamics.

In addition to the loss-of-function (LOF) phenotype, overexpression of either isoform of MISO resulted in significant mitochondrial fragmentation (**Fig. 2e-g**). Both isoforms were also observed to form comparable mitochondrial subdomains (**Supplementary Fig. 2p**), suggesting that they share similar molecular functions. Based on these similarities, we primarily utilized the long isoform of MISO in subsequent studies and referred to it simply as MISO, unless otherwise specified.

To investigate how MISO loss impacts mitochondrial dynamics, we analyzed the protein levels of key regulators involved in mitochondrial fission and fusion by Western blotting. Notably, mitochondrial fission protein 1 (FIS1) was significantly decreased in MISO-KO cells (**Fig. 2h-i**). Previous studies showed that FIS1 and dynamin-related protein 1 (DRP1) are specifically responsible for the periphery fission to generate small daughter mitochondria[9, 10]. We then examined DRP1's mitochondrial targeting in both wild-type (WT) and MISO-KO cells. Consistent with previous report, the number of DRP1 puncta on mitochondria was significantly

lower in MISO-KO cells compared to WT cells (**Fig. 2j-k**), suggesting that the hyper-fusion phenotype may result from impaired DRP1 recruitment. Conversely, overexpression of MISO led to mitochondrial fragmentation, likely through enhanced DRP1 recruitment. To test this hypothesis, we knocked down DRP1 and observed that it significantly suppressed the mitochondrial fragmentation caused by MISO overexpression (**Fig. 2l, Supplementary Fig. 2q-r**). These findings suggest that MISO promotes mitochondrial fission by the regulation of FIS1 and DRP1.

The MISO-Enriched Mitochondrial Subdomain (MEMS) plays dual roles in regulating mitochondrial dynamics.

The most prominent characteristics of MISO is its ability to generate MISO-enriched subdomains on mitochondria, observed consistently in both *Drosophila* and different mammalian cells, including U2OS, HeLa, Huh7, A549, PLC, and HEK293T (**Fig.1d, Fig3.a, Supplementary Fig. 3a**). To rule out the possibility that these subdomain formations are artifacts of tag fusion, we developed a polyclonal antibody against MISO. This antibody successfully detected overexpressed MISO but unfortunately not MISO expressed at endogenous levels (**Supplementary Fig. 3b**). Nevertheless, using this antibody, we confirmed that expressing untagged MISO in U2OS cells still results in the formation of similar mitochondrial subdomains (**Supplementary Fig. 3c**). These findings indicate that the generation of these subdomains is an intrinsic property of MISO and not an artifact of tag fusion. We previously demonstrated that endogenous MISO forms subdomains in *Drosophila* (**Fig. 1i**). To tested whether endogenous MISO also form similar subdomains in mammals, we generated knocked-in mice with a 3×Flag tag inserted at the C-terminus of mMISO (mouse MISO) (**Supplementary Fig. 4a**). Western blotting confirmed mMISO expression across multiple mice organs, with particularly high levels in energy-demanding tissues such as the brain, kidney, and brown fat (**Supplementary Fig. 4b**). To visualize mMISO localization, we isolated mouse embryonic fibroblasts (MEFs) from these mMISO-3xFlag knock-in mice and stained the cells with anti-Flag antibody. Our data showed that mMISO-3×Flag localizes to mitochondria and enriches in distinct subdomains, closely resembling those observed in *Drosophila* (**Fig. 3b**). These findings suggested that MISO can form mitochondrial subdomains at endogenous levels

in mammals. Given the unique characteristics of these structures, we decided to refer to them as MEMS (**M**ISO-**E**nriched **M**itochondria **S**ubdomain).

We further investigated the relationship between MISO protein levels and the formation of MEMS using a Tet-On inducible system. Notably, MEMS were detectable at the very onset of induction, even when MISO levels on the rest of the mitochondria were barely perceptible (**Fig. 3c, Supplementary Fig. 5**). As MISO levels increased, the intensity of MISO on regular mitochondria reached a plateau, while the number of MEMS continued to increase proportionally with MISO protein levels (**Fig. 3c, Supplementary Fig. 5**). These data suggest an interesting linear relationship between MEMS number and MISO protein level, suggest the biological effect of MISO may correlated with the presence of MEMS.

Recent studies have demonstrated that the mitochondrial inner membrane can herniate into the cytosol during mitophagy [15, 16], prompting us to examine the precise localization of MISO within and outside the MEMS region using STED super-resolution imaging. Our analysis revealed that the MISO signals, both within MEMS and in regular mitochondria, colocalized with the inner membrane marker ATP5a and were encapsulated by the outer membrane marker TOMM20 (**Fig 3. d-f, Supplementary Fig. 6a-c**). However, a small subset of MISO signals in MEMS (about 5 %) exhibited exceptions, which we will discuss in the following section. This is further supported by the proteinase protection assays with purified mitochondria (**Supplementary Fig. 6d-f**), which confirmed the integrity of the outer membrane in the majority of MEMS regions.

To identify proteins enriched in mitochondrial-derived vesicles (MEMS), we immunoprecipitated MISO from cell lysates and performed liquid chromatography-tandem mass spectrometry (LC-MS/MS) analysis (**Fig. 3g**). Candidate proteins were selectively validated using immunostaining with available antibodies (**Supplementary Fig.7**). Among them, prohibitin 1 and 2 (PHB1, PHB2) emerged as the most enriched proteins associated with MEMS (**Fig.3h, Supplementary Fig.8a**). Immunoprecipitation experiments confirmed the interaction between MISO and both PHB1 and PHB2, with notably stronger binding observed

for PHB2 (**Fig.3i**). PHB1 and PHB2 are inner mitochondrial membrane proteins that function together as a heterodimer in mitochondrial membrane organization [17]. Given their enrichment in MEMS, we investigated whether MEMS formation depends on PHBs. However, knocking down either PHB1 or PHB2 did not affect MEMS triggered by MISO expression, suggesting that PHBs are not required for MEMS formation (**Supplementary Fig. 8b-c**).

PHBs have been found to regulate of mitochondrial dynamics through several mechanisms, including binding and organizing the mitochondrial phospholipid cardiolipin, regulating the processing of the mitochondrial fusion protein optic atrophy 1 (OPA1), and interacting with dynamin-related protein 1 (DRP1) [18-20]. Since endogenous PHBs are enriched in MEMS (**Supplementary Fig.8a**), we tested whether the formation of MEMS result in the mitochondrial fragmentation. First, we confirmed that the number of MEMS in cells is inversely correlated with the average mitochondrial length (**Fig. 3j, Supplementary Fig.9**). As previous live-cell imaging study showed that different mechanisms govern the peripheral and midzone fission of mitochondria[9], we examined the relative location of MEMS within the mitochondria. Notably, while MEMS can be found both at the midzone and terminals of mitochondria, they exhibited a strong preference for peripheral localization (**Fig. k-l**). More interestingly, peripheral fission has been shown to be regulated through a unique FIS1-DRP1-dependent mechanism [9], which closely resembles the mechanism we identified for MISO. These findings led us to investigate whether the localization of MEMS on mitochondria correlates with fission events.

To study the real-time dynamics of MEMS, we initially attempted to fuse MISO with GFP or SNAP tags for live imaging. However, GFP fusion to either the N-terminus, C-terminus, or internal linker regions of MISO either blocked MEMS formation or caused MISO to translocate to the ER (data not shown). Nevertheless, the strong association of PHBs with MISO provided an alternative approach. While expressing PHB2-GFP alone uniformly labels mitochondria, it becomes highly concentrated in MEMS when co-expressed with MISO (**Supplementary Fig. 10a**). Therefore, we utilized PHB2-GFP to visualize the dynamics of MEMS in live cells. Live imaging revealed that although hMEMS can form at either the midzone or terminals of

mitochondria, MEMS formed at the midzone tend to move along the mitochondrion and eventually stabilize at the terminals (**Fig. 3m, Supplementary Fig. 10b, Supplementary Videos 1**). This observation explains why MEMS are more enriched at mitochondrial terminals.

We further investigated the spatiotemporal relationship between mitochondrial fission and MEMS. Our data revealed that mitochondria are twice as likely to undergo fission in regions close to MEMS structures (within 1 micron) (**Fig. 3n-o, Supplementary Videos 2**). Given that MEMS are predominantly located at the periphery of mitochondria, we propose that MEMS formation facilitates peripheral fission events. Indeed, we observed clear separation of MEMS from mitochondria, generating small fragments consistent with previous report [9, 10](**Supplementary Fig. 10c, Supplementary Videos 3**). Interestingly, we also observed that mitochondria with MEMS at their termini showed a significantly reduced likelihood (up to 90%) of fusing with other mitochondria, suggesting that MEMS also inhibit fusion (**Fig. 3p-q, Supplementary Videos 4**). We further validated this inhibitory effect using polyethylene glycol (PEG)-mediated cell fusion experiment [21]. Cells overexpressing MISO exhibited significantly reduced mitochondrial mixing after induced cell fusion (**Fig. 3r, Supplementary Fig. 10d**). Finally, we found inner membrane fusion protein OPA1 were exclude from MEMS but the outer membrane protein Mitofusin 2 (MFN2) was not affected (**Supplementary Fig. 10e-f**), suggesting MEMS inhibit fusion likely through OPA1 regulation. Collectively, these results indicate that MEMS serve as platforms for regulating mitochondrial dynamics by promoting fission and inhibiting fusion.

Previous studies have shown that mitochondrial fission is associated with contact sites between mitochondria and other organelles, such as the ER, Golgi, and lysosomes [3, 4, 22, 23]. To determine whether MEMS correlate with organelles other than mitochondria, we measured the spatial relationship between MEMS and various organelles. Our data indicated that, in addition to mitochondria, MEMS show a moderate association with the ER compared to other organelles (**Supplementary Fig.11**). However, the functional significance of this association remains to be determined through future functional studies.

MEMS associate and regulate mtDNA homeostasis.

Our proteomic analysis revealed that proteins involved in mitochondrial nucleoid formation are enriched in MEMS, including Poly ADP-Ribose Polymerase 1 (PARP1), Tu Translation Elongation Factor (TUFM), Single-Stranded DNA-Binding Protein 1 (SSBP1), Ribosomal Protein S3 (RPS3), ATPase family AAA domain-containing protein 3A (ATAD3A), and Mitochondrial Ribosomal Protein S27 (MRPS27) (**Fig. 3g**). Immunostaining of the major mitochondrial DNA (mtDNA) binding protein Mitochondrial transcription factor A (TFAM) showed mtDNA nucleoids are enriched in MEMS region (**Supplementary Fig. 12a**). Co-localization studies using antibodies against DNA and the mtRNA-associated protein FAST kinase domains containing 2 (FASTKD2) further supported the close association of mitochondrial nucleoids with MEMS (**Fig. 4a-b, Supplementary Fig.12b**). Live-cell imaging of MEMS labeled with PHB1-mCherry also showed strong covariation with the mitochondrial nucleoids labeled by PicoGreen (**Fig. 4c, Supplementary Fig. 12c, Supplementary Video 5**). EdU labeling assay demonstrated that these MEMS-associated nucleoids are actively replicating (**Supplementary Fig. 12d**). Additionally, we observed that SSBP1, a core mtDNA replication factor [24], associated with MEMS and physically interacts with MISO, as shown by both immunostaining and immunoprecipitation assays (**Supplementary Fig. 12e-f**). These findings suggest that MISO may recruit mitochondrial nucleoids to MEMS through its interaction with SSBP1.

Recently, a mitochondrial fusion inhibitor MTFP1 was discovered to regulate mtDNA degradation by participating in the formation of mitochondrial subdomains enriched in PHBs. These subdomains eventually separate from the main mitochondria through peripheral fission, forming a specialized mitochondrial population called small MTFP1-enriched mitochondria (SMEM), which are targeted for lysosomal degradation [10]. We found strong co-localization of MISO, MTFP1 and PHB2 within MEMS (**Fig. 4d**). Immunoprecipitation experiments further confirmed a physical interaction between MISO and MTFP1 (**Fig. 4e**). Increased ROS production and decreased membrane potential have been reported to mark mitochondria for degradation. And we found increased mitochondrial ROS levels (indicated by MitoSOX) and reduced membrane potential (indicated by TMRM) in MEMS (**Fig. 4f**), similar to previous

reports on MTFP1-enriched subdomains. Consistently, Seahorse assays and membrane potential measurements using the dye TMRM revealed that both OXPHOS activity and membrane potential were elevated in MISO-KO cells but reduced in MISO-overexpressing cells (**Supplementary Fig.13**). Furthermore, both PHB2 and MTFP1 have been shown to function as mitochondrial inner membrane receptors for the autophagosome-associated protein LC3 [10, 25], suggesting that MEMS may be involved in mitophagy. Indeed, similar to SMEM, we observed that MISO-bearing vesicles exhibited clear outer membrane breakage (marked by TOMM20) starting at the MEMS region (**Fig. 4g**). Notably, this outer membrane breakage was occasionally observed at the MEMS region even before their separation from filamentous mitochondria through peripheral fission (**Supplementary Fig. 14**). This finding indicates that MEMS are actively engaged in the mitophagic process, potentially serving as sites for selective mitochondrial degradation. Finally, these MISO-positive small mitochondrial fragments contain mtDNA and were found to associate with autophagy markers LC3 and Lysosome-associated membrane protein 1 (LAMP1) (**Fig. 4h-i**), supporting that they are trafficked to autophagic and lysosomal organelles. Collectively, these data showed MEMS and the previously identified MTFP1-enriched subdomain are the same structure.

To study the role of MISO in mtDNA homeostasis, we examined U2OS cells with MISO knocked out. MISO-KO cells exhibited significantly increased mtDNA nucleoid staining compared to wild-type (WT) cells without much effect on the size of nucleoid (**Fig.4j-l**). Quantitative PCR analysis confirmed that the relative mtDNA copy number (mtDNA CN) to nuclear DNA was higher in MISO-KO cells (**Fig. 4m**). Consistent with these findings, primary hepatocytes and MEFs isolated from mMISO-KO mice also showed significantly elevated mtDNA CN compared to those from WT mice (**Supplementary Fig.15a-b**). A similar increase in mtDNA CN was observed in the interscapular brown adipose tissue (iBAT) and inguinal white adipose tissue (iWAT) of mMISO-KO mice (**Supplementary Fig.15c**). Conversely, overexpressing MISO in U2OS cells led to a reduction in mtDNA CN (**Fig. 4n**). These results collectively demonstrate that MISO regulates mtDNA homeostasis both *in vitro* and *in vivo*.

Previous studies have shown that mtDNA damage, such as treatment with ethidium bromide

(EB)—which interferes with mtDNA replication and promotes nucleoid removal—induces the formation of SMEM [10, 26]. However, mutations in MTFP1 do not prevent SMEM formation after EB treatment, suggesting that the key sensor of mtDNA damage and organizer of these mitochondrial subdomains remains unidentified. Interestingly, using MEF cells derived from mMISO-Flag knock-in mice, we found that EB treatment significantly increased mMISO protein levels up to threefold, while the levels of other SMEM or MEMS markers, such as PHBs, remained unchanged (**Fig. 4o-p**). The mRNA level of MISO remained constant during treatment, suggesting that this induction likely occurs through post-transcriptional regulation (**Fig. 4p**). More importantly, MISO-KO completely blocked the formation of EB-induced PHB-enriched mitochondrial subdomains in U2OS cells (**Fig. 4q-r**). Additionally, MISO knockout did not affect the levels of MTFP1 or PHBs, indicating that the loss of these subdomains is likely directly due to the absence of MISO (**Fig. 4s, Supplementary Fig. 15d**). In summary, our data demonstrate that MISO is a key organizer of mitochondrial subdomains that regulate mtDNA homeostasis and respond to mtDNA damage.

Oligomerization of MISO drives MEMS formation by promoting intermembrane contacts.

To investigate the molecular mechanism underlying MISO-induced MEMS structures, we used transmission electron microscopy (TEM) and found that MISO overexpression resulted in significant cristae reduction. The inner mitochondrial membrane formed multiple layers that closely adhered to the outer membrane (**Fig. 5a, Supplementary Fig. 16a**). To test this, we stained the inner membrane with 10-N-nonyl acridine orange (NAO), a fluorescent probe that binds to the inner membrane specific lipid cardiolipin in live cells [27, 28]. NAO signal was highly condensed within MISO-induced MEMS (marked by PHB1-mCherry) (**Fig. 5b-c, Supplementary Fig. 16b**), suggesting an aggregation of mitochondrial inner membranes. Moreover, immunostaining for key regulators of cristae organization, including MIC60, ATP5a, and OPA1[29, 30], revealed their exclusion from the MEMS domain (**Fig. 5d, Fig. Supplementary Fig. 10e**). This observation further supports the idea that MEMS lack cristae junctions (organized by the MICOS complex) and cristae rims (organized by ATP synthase), consistent with the phenotype of collapsed inner membranes. Meanwhile, the overall levels of

these proteins remained unchanged (**Supplementary Fig. 16c-d**). Collectively, these findings suggest that MEMS arise from localized collapses of the inner mitochondrial membrane.

To further elucidate how MISO promotes the formation of multilayered membrane structures, we tried to map its topology within membrane. We combined TEM with ascorbate peroxidase (APEX) labeling [13]. APEX catalyzes the polymerization of diaminobenzidine (DAB) into a high electron-density precipitate, which can be visualized under an electron microscope. By fusing APEX to either the N- or C-terminus of MISO, we determined that the N-terminus of MISO faces the mitochondrial intermembrane space, while the C-terminus is oriented toward the mitochondrial matrix (**Figure 5e-f**). This topological arrangement is also supported by the proteinase protection assays, in which the Flag tag attached to the C-terminus of MISO was protected from exogenous proteases by the integrity of the inner mitochondrial membrane (**Supplementary Fig. 6f**). Notably, when the relatively large APEX (28 kDa) was fused to the C-terminus of MISO, the resulting MISO-APEX lost its ability to induce MEMS formation or cause mitochondrial fragmentation (**Fig. 5e-g**). In contrast, fusing small tags, such as Flag and HA, to the C-terminus did not interfere with MISO's functionality. Based on these observations, we hypothesize that MISO's functional state requires the C-terminus to be integrated into a densely packed protein complex, which is essential for its activity.

Indeed, a recent study has suggested that MISO is a member of the prohibitin-stomatin family [31], which belongs to the ancient SPFH (Stomatin, Prohibitin, Flotillin, and HflK/C) family found in both prokaryotic and eukaryotic cells [32]. A hallmark feature of this protein family is their propensity for self-oligomerization into large membrane-spanning or membrane-anchored complexes [33]. To determine whether MISO exhibits similar oligomerization behavior, we performed disuccinimidyl glutarate (DSG) crosslinking experiments. Upon DSG treatment, clear dimer and oligomer bands were observed (**Fig. 5h**). Immunoprecipitation experiments also confirmed that MISO binds to itself (**Fig. 5i**). Based on the topology and biochemical properties of MISO, we hypothesized that MEMS are formed through trans-interactions between the C-termini of MISO proteins located on opposing mitochondrial inner membranes.

One way to test this hypothesis would be to reconstitute MISO-containing liposomes *in vitro*. However, attempts to obtain high quality soluble full-length MISO protein from both prokaryotic and eukaryotic expression systems were unsuccessful (data not shown). Instead, we decided to test our hypothesis within a cellular context. We constructed an artificial protein, OMM-MISO(C), by replacing the N-terminus and transmembrane region of MISO with the mitochondrial outer membrane localization sequence from TOMM20. This modification targeted the C-terminal domain of MISO to the outer mitochondrial membrane (**Fig. 5j-k**). Expression of OMM-MISO-Cterm in cells promoted robust trans-interactions between mitochondria, resulting in large, aggregated mitochondria in both U2OS and HEK293T cells (**Fig. 5l-m, Supplementary Fig. 17**). This outcome supports our hypothesis that the MISO(C) mediates inter-membrane contacts. To further investigate whether the MISO(C) is sufficient for its biological function, we fused the MISO(C) with the inner membrane localization sequence from mitochondrial chaperone BCS1 to generate IMM-MISO(C) (**Fig. 5j-k**). Expression of IMM-MISO(C) recapitulated the formation of MEMS-like microdomains and induced mitochondrial fragmentation (**Fig. 5n-o**). Collectively, our data demonstrate that MISO promotes trans-associations between mitochondrial inner membranes through its C-terminal domain, leading to cristae collapse and the generation of distinct mitochondrial inner membrane subdomains.

Discussion

Previous research has established a connection between mitochondrial dynamics and mtDNA homeostasis. Mutations affecting fusion and fission machinery have been found to alter the size and number of mitochondrial nucleoids [34]. Fission events have been associated with mtDNA replication and its subsequent segregation, as the location and replication of mitochondrial nucleoids is regulated by endoplasmic reticulum (ER)-mitochondria contact mediated mitochondrial fission[22, 23]. Moreover, evidence suggests that mitochondrial fusion plays an essential role in mtDNA replication. Mutations in components of the fusion machinery consistently lead to reductions in mtDNA copy numbers [34], potentially due to decreased levels of key replisome enzymes such as single-stranded DNA-binding protein 1 (SSBP1) and mitochondrial polymerase γ (POLG) [35]. Blocking fission has also been shown to increase

mtDNA levels and the retention of mutant mtDNA, possibly through inhibition of mitophagy [34, 36]. Several molecules have been proposed to link mitochondrial morphology with mtDNA nucleoid organization. Cardiolipin, a phospholipid unique to the inner mitochondrial membrane, has been found to bind nucleoids and regulates mitochondrial inner membrane fusion[37, 38]. Additionally, the MICOS complex, (mitochondrial contact site and cristae organizing system) has been implicated in regulation of both mitochondrial dynamics and mtDNA nucleoid organization through interaction with Miro1[39]. However, there remains a paucity of information on how these molecules are spatially and structurally organized to integrate mitochondrial dynamics with mtDNA maintenance. Our study provides the missing molecular and structural linkage between mitochondrial dynamics and mtDNA maintenance, by showing that MISO orchestrates the formation of a distinct mitochondrial subdomain, MEMS, regulating both mitochondria morphology and mtDNA copy number (**Supplementary Fig. 18**).

While our findings provide valuable insights, they also raise several intriguing questions for future studies. First, in-depth biochemical studies are still required to fully elucidate the molecular function of MISO. We have demonstrated that MEMS formation is mediated by the oligomerization of MISO via its C-terminus, which facilitates contact between opposing inner mitochondrial membranes. However, relocating the C-terminus of MISO to the outer membrane does not induce similar subdomain formation, suggesting that additional protein partners within the inner membrane or matrix may be required for MEMS establishment. Experiments utilizing reconstituted MISO-containing liposomes could provide critical insights in this regard. Additionally, the precise molecular mechanisms by which MISO regulates FIS1 and OPA1 remain unclear, which may be dissected through specific MISO mutants that lost particular function. To dissect the domains or residues responsible for MEMS organization, fusion and fission regulation, and mtDNA nucleoid association, we have tested various truncations and point mutations of evolutionarily conserved residues in MISO. However, deletions within the C-terminal domain of MISO consistently impair its mitochondrial localization, and no point mutations have significantly altered MISO's function in our assays. These observations highlight the complexity of MISO's role and underscore the need for more sophisticated approaches to unravel its molecular mechanisms.

Beyond elucidating the molecular properties of MISO, understanding its regulation by upstream signaling pathways is also essential for a comprehensive understanding of its function. Both flies and mice lacking MISO are viable and fertile, suggesting that MISO and MEMS might play a more significant role under pathological conditions. This hypothesis is supported by observations that ErB-induced mtDNA damage significantly promotes MEMS formation through the upregulation of MISO. Notably, previous study demonstrated that MTFP1, the major component of MEMS, is translationally controlled by mammalian target of rapamycin (mTOR) signaling [40]. It is plausible that MISO's expression or activity could be modulated by signaling cascades in response to cellular stress or damage. Indeed, recent genome-wide analyses have revealed that MISO is associated with diseases such as cancers [41] and brain-related disorders, including common epilepsies and alcohol dependence [42, 43], consistent with its high expression in the mouse central nervous system (CNS). Therefore, further investigations under stressed or sensitized conditions may offer valuable insights into the regulatory pathways governing MISO and its functional significance in such contexts, particularly in response to mtDNA damage.

Author Contributions: Conceptualization, experiments design by L.H., Y.Z., and Q. Z.; experiments performance, data collection and analysis by Y.Z., X.W., Y.X., and X. G.. All authors have read and agreed to the published version of the manuscript.

Data Availability Statement: All data generated or analyzed in this study are included in the main text or the Supplementary materials. The raw data generated in this study are provided in the Source Data file in this paper. The protein mass spectrometry data has been deposited on the ProteomeXchange PRIDE database with the identifier: PXD057461.

Acknowledgments: funding for this work is from the National Natural Science Foundation of China (No. 32470754), the startup funds from USTC to L.H. We thank Dr. Norbert Perrimon

and Dr. Richard Binari at Harvard Medical School for support of the initial genetic screen in *Drosophila*. We thank the Cryo-EM Center in University of Science and Technology of China and the Core facility of Harvard Medical School for preparation of ultrathin sections and TEM operation.

Conflicts of Interest: The authors declare no conflict of interest.

References

1. Suomalainen, A. and J. Nunnari, *Mitochondria at the crossroads of health and disease.* Cell, 2024. **187**(11): p. 2601-2627.
2. Benador, I.Y., et al., *Mitochondria Bound to Lipid Droplets Have Unique Bioenergetics, Composition, and Dynamics that Support Lipid Droplet Expansion.* Cell Metab, 2018. **27**(4): p. 869-885 e6.
3. Wong, Y.C., D. Ysselstein, and D. Krainc, *Mitochondria-lysosome contacts regulate mitochondrial fission via RAB7 GTP hydrolysis.* Nature, 2018. **554**(7692): p. 382-386.
4. Nagashima, S., et al., *Golgi-derived PI(4)P-containing vesicles drive late steps of mitochondrial division.* Science, 2020. **367**(6484): p. 1366-1371.
5. Ryu, K.W., et al., *Cellular ATP demand creates metabolically distinct subpopulations of mitochondria.* Nature, 2024. **635**(8039): p. 746-754.
6. Hughes, A.L., et al., *Selective sorting and destruction of mitochondrial membrane proteins in aged yeast.* Elife, 2016. **5**.
7. Schuler, M.H., et al., *Mitochondrial-derived compartments facilitate cellular adaptation to amino acid stress.* Mol Cell, 2021. **81**(18): p. 3786-3802 e13.
8. Li, X., et al., *Mitochondria shed their outer membrane in response to infection-induced stress.* Science, 2022. **375**(6577): p. eabi4343.
9. Kleele, T., et al., *Distinct fission signatures predict mitochondrial degradation or biogenesis.* Nature, 2021. **593**(7859): p. 435-439.
10. Tabara, L.C., et al., *MTFP1 controls mitochondrial fusion to regulate inner membrane quality control and maintain mtDNA levels.* Cell, 2024. **187**(14): p. 3619-3637 e27.
11. He, L., et al., *In vivo study of gene expression with an enhanced dual-color fluorescent transcriptional timer.* Elife, 2019. **8**.
12. Hao, D., et al., *AC3-33, a novel secretory protein, inhibits Elk1 transcriptional activity via ERK pathway.* Mol Biol Rep, 2011. **38**(2): p. 1375-82.
13. Rhee, H.W., et al., *Proteomic mapping of mitochondria in living cells via spatially restricted enzymatic tagging.* Science, 2013. **339**(6125): p. 1328-1331.
14. Chen, C.L., et al., *Proteomic mapping in live Drosophila tissues using an engineered ascorbate peroxidase.* Proc Natl Acad Sci U S A, 2015. **112**(39): p. 12093-8.
15. Saunders, T.L., et al., *Exposure of the inner mitochondrial membrane triggers apoptotic mitophagy.* Cell Death Differ, 2024. **31**(3): p. 335-347.
16. McArthur, K., et al., *BAK/BAX macropores facilitate mitochondrial herniation and mtDNA efflux*

during apoptosis. Science, 2018. **359**(6378).

17. Oyang, L., et al., *The function of prohibitins in mitochondria and the clinical potentials.* Cancer Cell Int, 2022. **22**(1): p. 343.
18. Christie, D.A., et al., *Stomatin-like protein 2 binds cardiolipin and regulates mitochondrial biogenesis and function.* Mol Cell Biol, 2011. **31**(18): p. 3845-56.
19. Ban, T., et al., *Relationship between OPA1 and cardiolipin in mitochondrial inner-membrane fusion.* Biochim Biophys Acta Bioenerg, 2018. **1859**(9): p. 951-957.
20. Raut, G.K., et al., *Glucose starvation-induced oxidative stress causes mitochondrial dysfunction and apoptosis via Prohibitin 1 upregulation in human breast cancer cells.* Free Radic Biol Med, 2019. **145**: p. 428-441.
21. Pontecorvo, G., *Production of mammalian somatic cell hybrids by means of polyethylene glycol treatment.* Somatic Cell Genet, 1975. **1**(4): p. 397-400.
22. Lewis, S.C., L.F. Uchiyama, and J. Nunnari, *ER-mitochondria contacts couple mtDNA synthesis with mitochondrial division in human cells.* Science, 2016. **353**(6296): p. aaf5549.
23. Friedman, J.R., et al., *ER tubules mark sites of mitochondrial division.* Science, 2011. **334**(6054): p. 358-62.
24. Korhonen, J.A., et al., *Reconstitution of a minimal mtDNA replisome in vitro.* EMBO J, 2004. **23**(12): p. 2423-9.
25. Wei, Y., et al., *Prohibitin 2 Is an Inner Mitochondrial Membrane Mitophagy Receptor.* Cell, 2017. **168**(1-2): p. 224-238 e10.
26. Leibowitz, R.D., *The effect of ethidium bromide on mitochondrial DNA synthesis and mitochondrial DNA structure in HeLa cells.* J Cell Biol, 1971. **51**(1): p. 116-22.
27. Garcia Fernandez, M.I., D. Ceccarelli, and U. Muscatello, *Use of the fluorescent dye 10-N-nonyl acridine orange in quantitative and location assays of cardiolipin: a study on different experimental models.* Anal Biochem, 2004. **328**(2): p. 174-80.
28. Fuentes, J.M. and P. Morcillo, *The Role of Cardiolipin in Mitochondrial Function and Neurodegenerative Diseases.* Cells, 2024. **13**(7).
29. Benaroya, H., *Mitochondria and MICOS - function and modeling.* Rev Neurosci, 2024. **35**(5): p. 503-531.
30. Caron, C. and G. Bertolin, *Cristae shaping and dynamics in mitochondrial function.* J Cell Sci, 2024. **137**(1).
31. Morgenstern, M., et al., *Quantitative high-confidence human mitochondrial proteome and its dynamics in cellular context.* Cell Metab, 2021. **33**(12): p. 2464-2483 e18.
32. Ma, C., et al., *Structural insights into the membrane microdomain organization by SPFH family proteins.* Cell Res, 2022. **32**(2): p. 176-189.
33. Browman, D.T., M.B. Hoegg, and S.M. Robbins, *The SPFH domain-containing proteins: more than lipid raft markers.* Trends Cell Biol, 2007. **17**(8): p. 394-402.
34. Sabouny, R. and T.E. Shutt, *The role of mitochondrial dynamics in mtDNA maintenance.* J Cell Sci, 2021. **134**(24).
35. Silva Ramos, E., et al., *Mitochondrial fusion is required for regulation of mitochondrial DNA replication.* PLoS Genet, 2019. **15**(6): p. e1008085.
36. Malena, A., et al., *Inhibition of mitochondrial fission favours mutant over wild-type mitochondrial DNA.* Hum Mol Genet, 2009. **18**(18): p. 3407-16.
37. Luevano-Martinez, L.A., et al., *Cardiolipin is a key determinant for mtDNA stability and*

segregation during mitochondrial stress. Biochim Biophys Acta, 2015. **1847**(6-7): p. 587-98.

38. Ban, T., et al., *Molecular basis of selective mitochondrial fusion by heterotypic action between OPA1 and cardiolipin.* Nat Cell Biol, 2017. **19**(7): p. 856-863.
39. Li, H., et al., *Mic60/Mitofilin determines MICOS assembly essential for mitochondrial dynamics and mtDNA nucleoid organization.* Cell Death Differ, 2016. **23**(3): p. 380-92.
40. Morita, M., et al., *mTOR Controls Mitochondrial Dynamics and Cell Survival via MTFP1.* Mol Cell, 2017. **67**(6): p. 922-935 e5.
41. Hu, F., et al., *Analysis of AC3-33 gene expression in multiple organ cancer and adjacent normal tissue by RNA in situ hybridization.* Oncol Lett, 2015. **9**(6): p. 2795-2798.
42. International League Against Epilepsy Consortium on Complex, E., *Genome-wide mega-analysis identifies 16 loci and highlights diverse biological mechanisms in the common epilepsies.* Nat Commun, 2018. **9**(1): p. 5269.
43. Zhang, J., et al., *Integrative Analysis of Proteome-wide Association Studies and Functional Enrichment Analysis to Identify Genes and Chemicals Associated with Alcohol Dependence.* J Addict Med, 2023. **17**(3): p. 319-325.

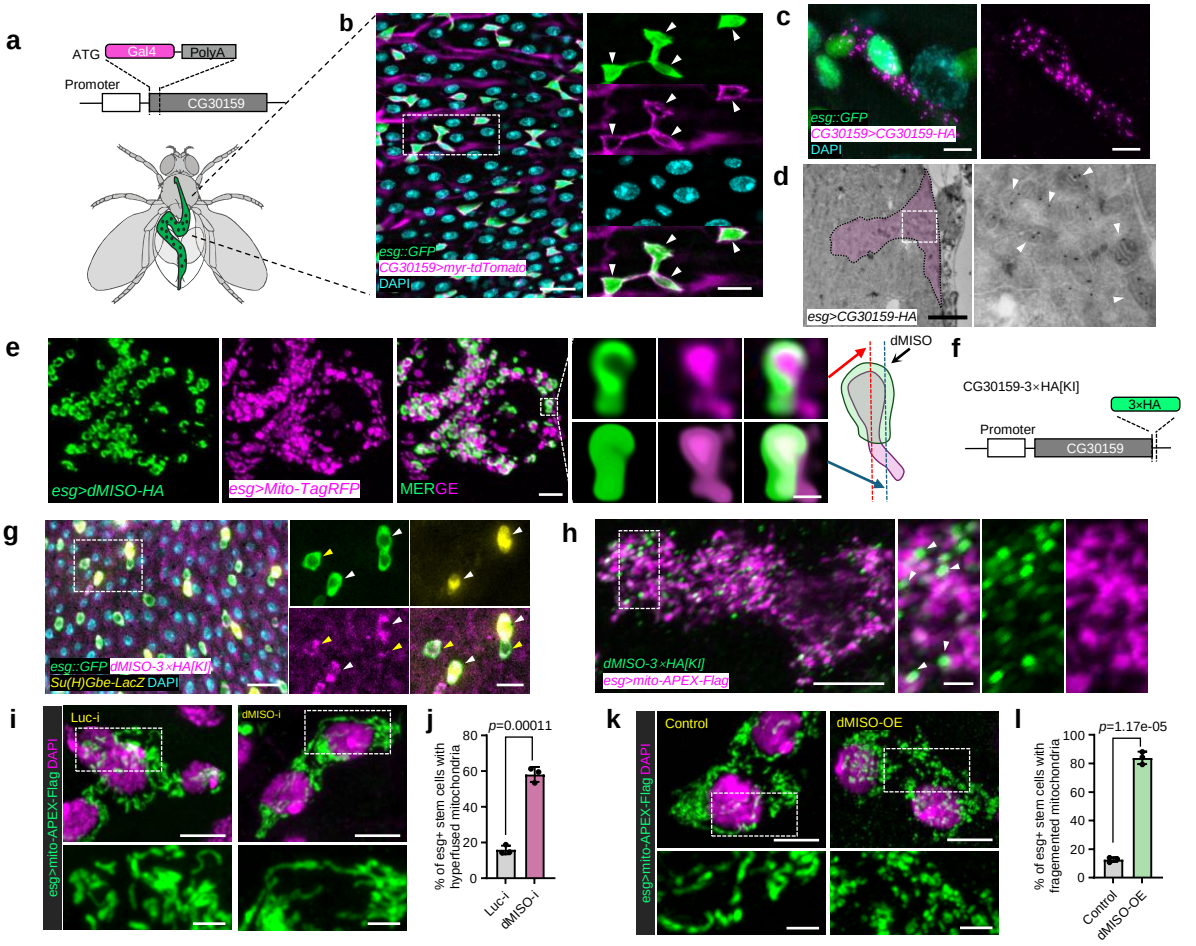

Fig. 1. *Drosophila* dMISO/CG30159 forms mitochondrial subdomains and regulates mitochondrial dynamics.

a-b. CG30159 is expressed in escargot (esg)-positive stem cells (green) in the adult fly intestine by the Gal4 knock-in element. Scale bars: main panels 20 μm, magnified insets 10 μm.

c. HA-tagged CG30159 in stem cells exhibits multiple punctate patterns. Scale bars: 5 μm.

d. Immuno-electron microscopy (EM) analysis of CG30159 (esg>CG30159-HA) localization in the *Drosophila* intestine. White arrowheads mark immunogold-labeled CG30159. The red pseudo-color indicates stem cells.

e. Representative images of CG30159 immunofluorescence staining in esg+ stem cells. Mito-TagRFP is used as a marker for mitochondria matrix. Scale bar: 2 μm. Magnified insets display the original data of a single subdomain of dMISO within mitochondria (upper panel) and corresponding 3D surface reconstructions (lower panel). Scale bar: 500 nm.

f. A diagram of CG30159 gene structure with 3×HA tag knock-in element.

g. Representative images showing endogenous dMISO protein expression in fly intestine. Yellow arrowheads indicate stem cells, and white arrowheads indicate enteroblasts. Scale bars: main panels 20 μm, magnified insets 10 μm.

g. Representative images showing endogenous dMISO protein expression in fly intestine. Yellow arrowheads indicate stem cells, and white arrowheads indicate enteroblasts. Scale bars: main panels 20 μm, magnified insets 10 μm.

h. Representative images depicting the localization of endogenous dMISO in intestinal stem cells. Scale bars: main panels 5 μm, magnified insets 1 μm.

i-j. Representative images (i) and corresponding quantifications (j) of mitochondrial morphology in Luc-i (RNAi) and dMISO-i esg+ stem cells within the fly intestines. Scale bars: main panels 5 μm, magnified insets 2 μm.

k-l. Representative images (k) and corresponding quantifications (l) of mitochondrial morphology in dMISO-OE (Overexpressed) esg+ stem cells within the fly intestines. Scale bars: main panels 5 μm, magnified insets 2 μm.

All data are presented as mean ± SD. j, l: unpaired two-tailed t-tests.

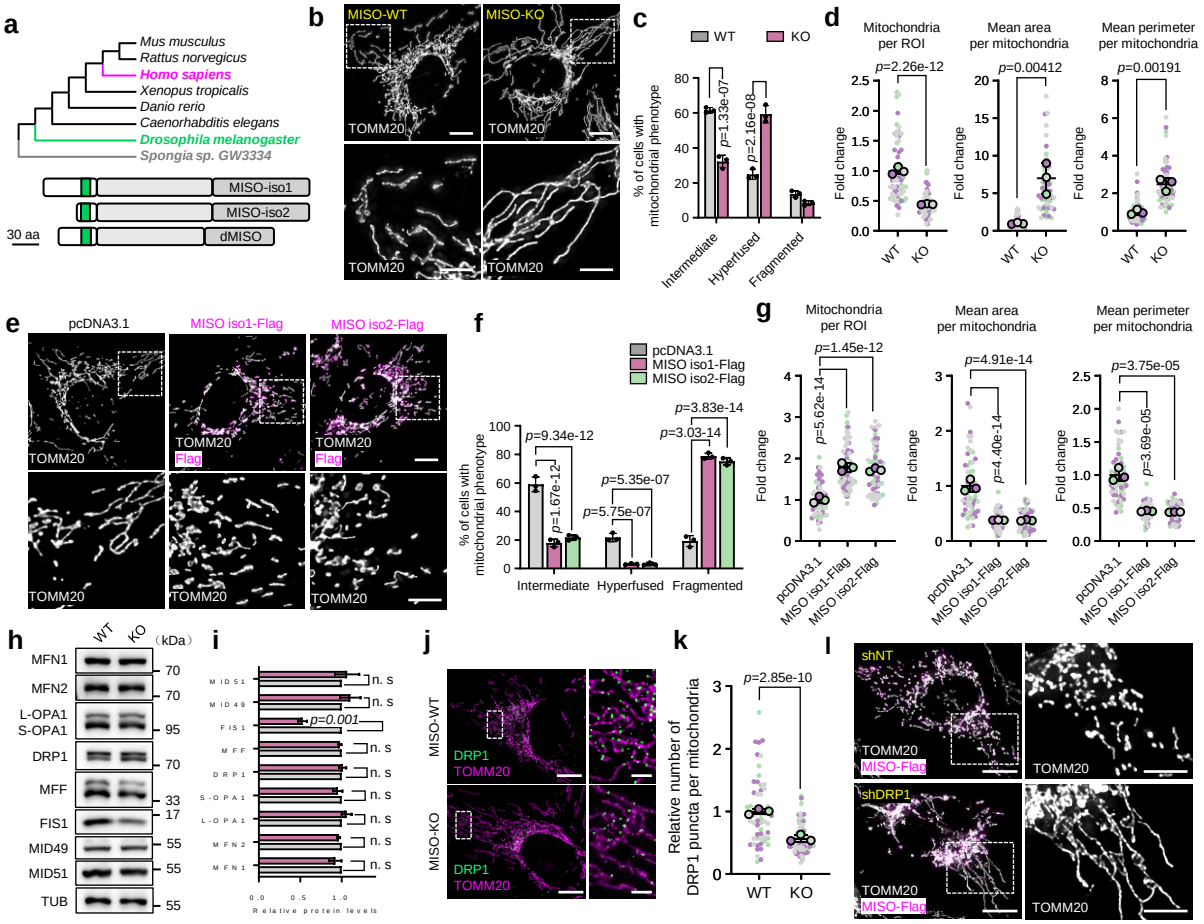

Fig. 2. MISO/C3orf33 forms mitochondrial subdomains and regulates mitochondrial dynamics.

a. MISO is evolutionarily conserved across major metazoan species, spanning from sea sponges to humans. The typical transmembrane (TM) domains are highlighted in green.

b-c. Representative images (b) and corresponding quantification (c) of mitochondrial morphology in wild-type (WT) and MISO-knockout (KO) U2OS cells. Scale bars: main panels 10 μm, magnified insets 5 μm.

d. Quantification of mitochondrial parameters from (b).

e-f. Representative images (e) and corresponding quantification (f) of mitochondrial morphology in U2OS cells overexpressing an empty vector (pcDNA3.1) , MISO isoform1-Flag or MISO isoform2-Flag. Scale bars: main panels 10 μm, magnified insets 5 μm.

g. Quantification of mitochondrial parameters from (e).

h-i. Representative immunoblots (h) and corresponding quantifications (i) of proteins involved in mitochondrial fission and fusion from WT and MISO-KO U2OS cells.

j. Representative images of DRP1 localization in WT and MISO-KO U2OS cells. Scale bars: main panels 10 μm, magnified insets 2 μm.

k. Quantification of DRP1 puncta on TOMM20-labeled mitochondria.

l. Representative images of mitochondrial morphology in U2OS cells expressing MISO-Flag and treated with the indicated shRNAs. NT: non-targeted. Scale bars: main panels 10 μm, magnified insets 5 μm.

All data are presented as mean ± SD. c, f: two-way ANOVA with Tukey's multiple comparisons test; d, k: two-tailed nested t test; g: nested ordinary one-way ANOVA with Tukey's multiple comparisons test; i: two-tailed unpaired t test. n. s: not significant.

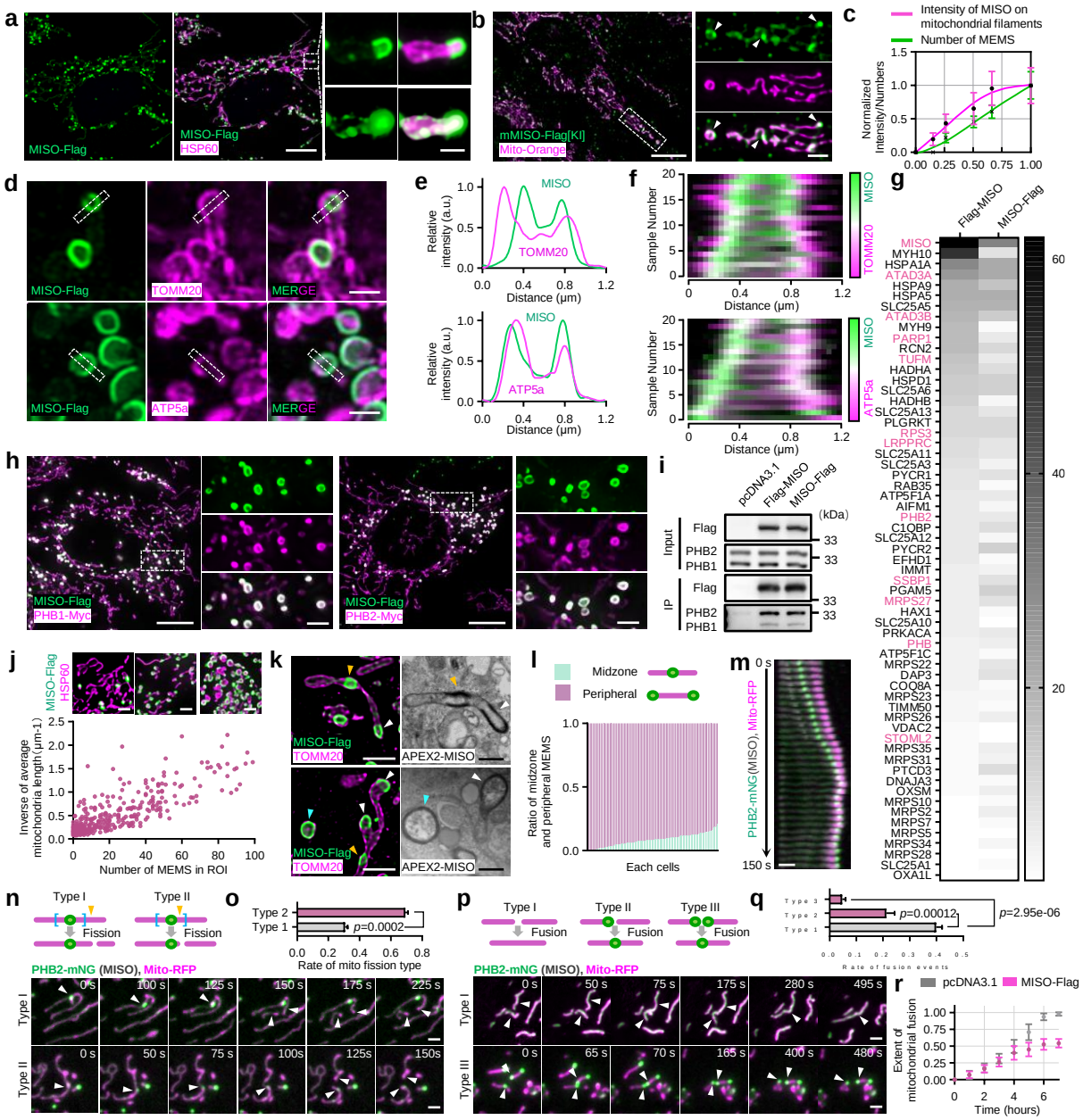

Fig. 3. MEMS play a dual role in regulating mitochondrial dynamics.

a. Representative images depicting the localization of MISO in U2OS cells. The insets highlight the raw data pertaining to the mitochondrial subdomains (upper panel) and feature 3D surface reconstructions (lower panel). Scale bars: main panels 10 μm, magnified insets 1 μm.

b. Representative images depicting the localization of endogenous MISO in MEFs. White arrowheads indicate mitochondrial subdomains. Scale bars: main panels 10 μm, magnified insets 2 μm.

c. The intensity of MISO on mitochondrial filaments and the number of MEMS (MISO-Enriched Mitochondria Subdomain) are plotted at varying levels of MISO expression.

d. Representative images confirming MEMS localization to the inner mitochondrial membrane in U2OS cells expressing MISO-Flag. Immunofluorescence staining was performed to detect the Flag epitope (green) and co-stained with TOMM20 (outer membrane, top panel, magenta) or ATP5a (inner membrane, bottom panel, magenta). Scale bars: 1 μm.

e. Line profiles showing fluorescent signals of each channel across MEMS marked by the dotted rectangles in (d).

f. Fluorescence colocalization analysis of MISO (green) in mitonchondrial subdomains with TOMM20 (top panel, magenta) or ATP5a (bottom panel, magenta).

g. Heatmap depicting the major mitochondrial protein of Flag-MISO and MISO-Flag interacomes analyzed via liquid chromatography-mass spectrometry (LC-MS). Color intensity reflects the number of identified peptides.

h. Fluorescence colocalization analysis of MISO with PHB1-Myc and PHB2-Myc. Scale bars: main panels 10 μm, magnified insets 2 μm.

i. Immunoblots of the indicated proteins from anti-Flag immunoprecipitation of HEK293T cells overexpressing either an empty vector (pcDNA3.1), Flag-MISO or MISO-Flag.

j. Representative images and scatter plot illustrating the association between mitochondrial length and the number of MEMS per ROI in cells expressing MISO-Flag Scale bars: 2 μm.

k. Representative fluorescence (left panel) and electron microscopy (right panel) images of midzone and peripheral MEMS in U2OS cells. Arrowheads: white for peripheral MEMS, yellow for midzone MEMS, and blue for isolated MEMS. Scale bar: fluorescence images 2 μm, EM images 500nm.

l. Histogram showing the distribution of midzone and peripheral MEMS proportions per cell in cells expressing MISO-Flag.

m. Kymograph depicting the migration of MEMS toward the mitochondrial periphery. Scale bar: 2 μm.

n. Representative time-lapse images of mitochondrial fission events in U2OS cells expressing MISO-Flag and PHB2-mNeoGreen (indicating MISO) (green) along with Mito-RFP (magenta). White arrowheads point to MEMS. Type I fission: Fission event occurring within a 0-1 μm range from the MEMS spot. Type II fission: Fission event occurring within a 1-2 μm range from the MEMS spot. Scale bar: 2 μm.

o. Quantitative evaluation of the rates of Type I and Type II mitochondrial fission events.

p. Representative time-lapse images of mitochondrial fusion events in U2OS cells expressing MISO-Flag and PHB2-mNeoGreen (indicating MISO) (green) along with Mito-RFP (magenta). White arrowheads point to MEMS. Type I fusion: Fusion between two mitochondrial termini without MEMS. Type II fusion: Fusion between two mitochondrial termini with MEMS present on one terminus. Type III fusion: Fusion between two mitochondrial termini with MEMS present on both termini. Scale bar: 2 μm.

q. Quantitative assessment of mitochondrial fusion probabilities across three types of encounter events.

r. Mitochondrial fusion kinetics were quantitatively analyzed by measuring the proportion of overlapping mitochondria relative to total mitochondrial content in at hybrid cells per time point.

All data are presented as mean ± SD. o: two-tailed unpaired t test; q: ordinary one-way ANOVA with Tukey's multiple comparisons test.

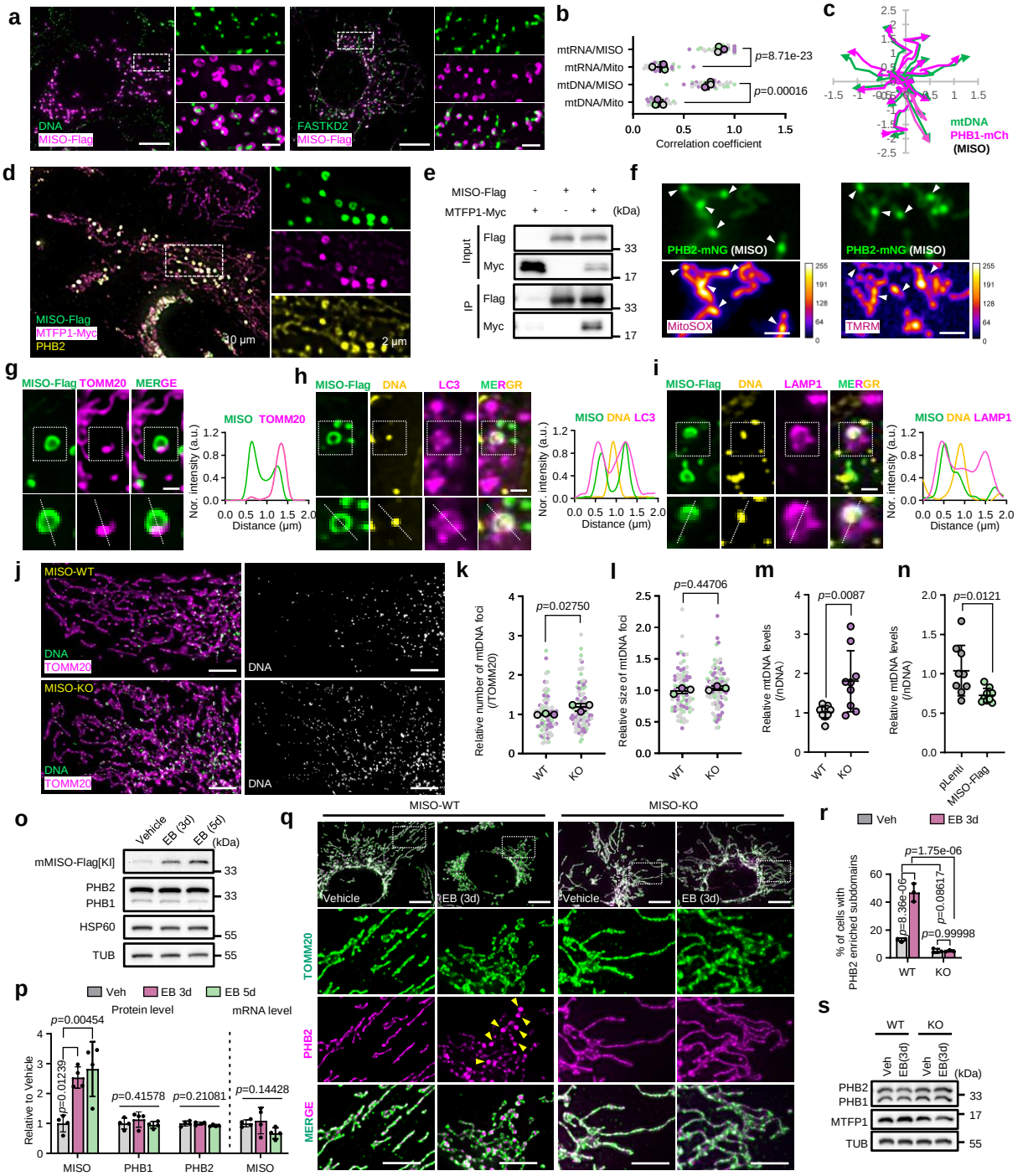
a
DNA
MISO-Flag
FASTKD2
MISO-Flag
b
mtRNA/MISO
mtRNA/Mito
mtDNA/MISO
mtDNA/Mito
p=8.71e-23
p=0.00016
Correlation coefficient
c
mtDNA
PHB1-mCh
(MISO)
d
MISO-Flag
MTFP1-Myc
PHB2
10 μm
2 μm
e
MISO-Flag
MTFP1-Myc
(kDa)
Input
IP
Flag
Myc
33
17
f
PHB2-mNG (MISO)
MitoSOX
TMRM
g
MISO-Flag TOMM20 MERGE
MISO TOMM20
Nor. intensity (a.u.)
Distance (μm)
h
MISO-Flag DNA LC3 MERGR
MISO DNA LC3
i
MISO-Flag DNA LAMP1 MERGR
MISO DNA LAMP1
j
MISO-WT
MISO-KO
DNA
TOMM20
k
Relative number of mtDNA foci (/TOMM20)
p=0.02750
WT
KO
l
Relative size of mtDNA foci
p=0.44706
m
Relative mtDNA levels (/nDNA)
p=0.0087
n
Relative mtDNA levels (/nDNA)
p=0.0121
pLenti
MISO-Flag
o
Vehicle
EB (3d)
EB (5d)
(kDa)
mMISO-Flag[KI]
PHB2
PHB1
HSP60
TUB
33
55
p
Veh
EB 3d
EB 5d
Protein level
mRNA level
Relative to Vehicle
p=0.00454
p=0.01239
p=0.41578
p=0.21081
p=0.14428
MISO
PHB1
PHB2
MISO
q
MISO-WT
MISO-KO
Vehicle
EB (3d)
TOMM20
PHB2
MERGE
r
Veh
EB 3d
% of cells with PHB2 enriched subdomains
p=1.75e-06
p=8.36e-06
p=0.08617
p=0.99998
WT
KO
s
WT
KO
Veh
EB(3d)
(kDa)
PHB2
PHB1
MTFP1
TUB
33
17
55

Fig. 4. MEMS regulate mtDNA homeostasis and are induced by mtDNA damage.

a. Representative images depicting the association between mtDNA or mtRNA (indicated by FASTKD2 staining) with MEMS in U2OS cells. Scale bars: main panels 10 μm, magnified insets 2 μm.

b. Quantification of correlation coefficient between MEMS and mtDNA or mtRNA in cells shown in (a) . n=30 cells were analyzed per group.

c. Migration paths of mitochondrial DNA (PicoGreen, green) and mCherry-PHB1 (representing MISO, red) were tracked using MTrack2 in Fiji software.

d. Representative images showing the colocalization of MISO, MTFP1, and PHB2. Scale bars: main panels 10 μm, magnified insets 2 μm.

e. Co-Immunoprecipitation with anti-Flag validate the interaction between MISO and MTFP1.

f. Representative images of U2OS cells expressing PHB2-mNeoGreen and MISO-Flag incubated with MitoSOX or TMRM. Scale bars, 2 μm.

g. Representative images and line profiles showing the absence of TOMM20 within MEMS. Scale bars, 1 μm.

h-i. Representative images and line profiles showing the presence of MEMS within autolysosome structures marked by LC3 (g) and LAMP1 (h). Scale bars, 1 μm.

j. Representative images of mtDNA and mitochondria in WT and MISO-KO U2OS cells. Scale bars, 5 μm.

k-l. Quantification of the number (j) and size (k) of mtDNA foci per ROI from (i).

m. qPCR analysis of mtDNA copy number in WT and MISO-KO U2OS cells. n = 6 independent experiments.

n. qPCR analysis of mtDNA copy number in U2OS cells expressing an empty vector (pLenti) or MISO-Flag**.** n= 6 independent experiments.

o. Representative immunoblots of indicated proteins from 3×Flag tag Knock-in MEFs incubated in the presence or absence of EB.

p. Quantification of indicated proteins and mRNA levels from (n).

q-r. Representative images (p) and corresponding quantifications (q) of PHB2-enriched microdomains (yellow arrows) in WT and MISO-KO U2OS cells incubated in the presence or absence of EB. Scale bars, 10 μm and 5 μm.

s. Representative immunoblots of indicated proteins from WT and MISO-KO U2OS cells incubated in the presence or absence of EB.

All data are presented as mean ± SD. b, k-l: two-tailed nested t test; m-n: two-tailed unpaired t test; p: ordinary one-way ANOVA with Tukey's multiple comparisons test; r: two-way ANOVA with Tukey's multiple comparisons test.

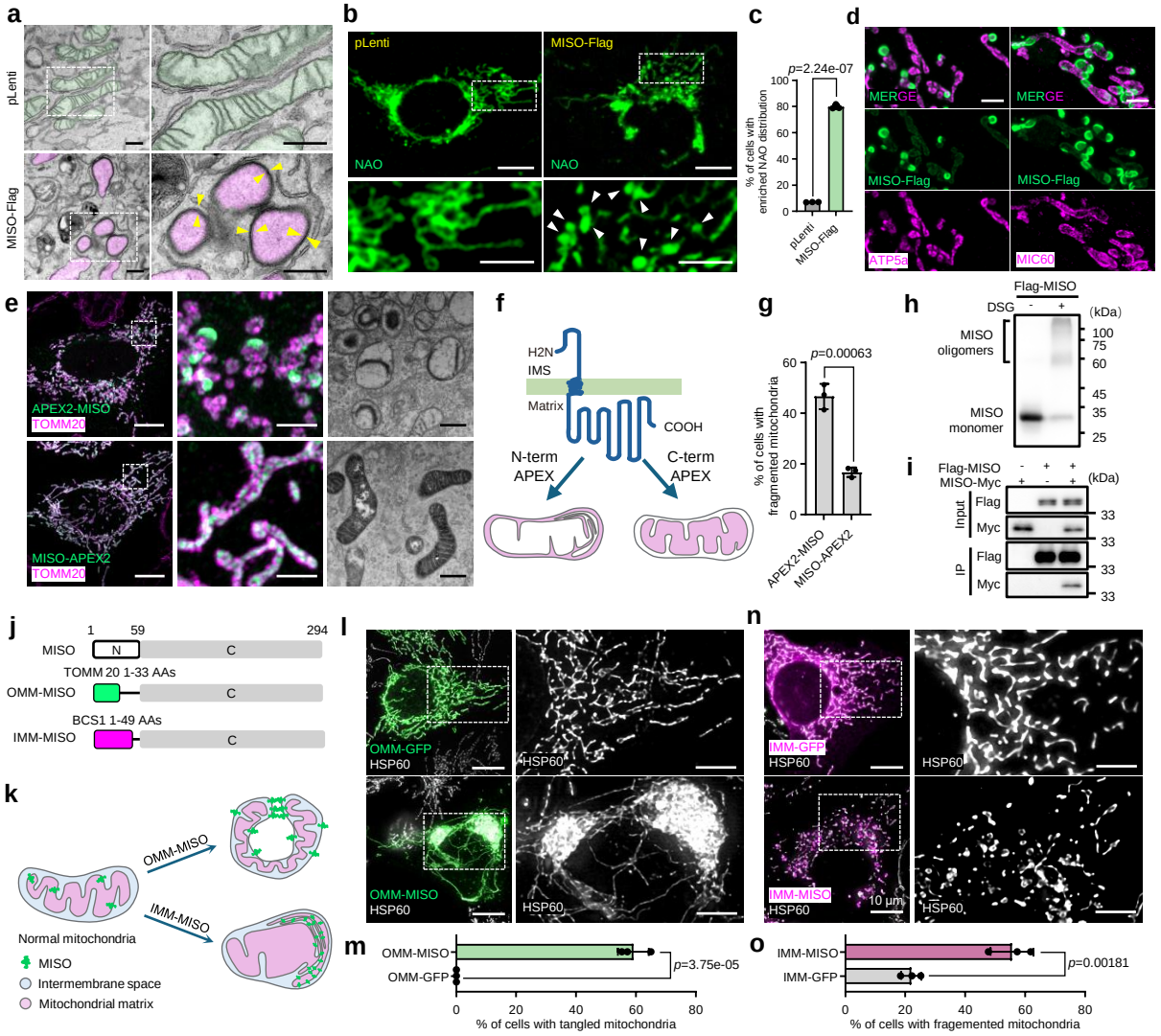

Fig. 5. Oligomerization of MISO drives MEMS formation by facilitating intermembrane contacts.

a. Representative TEM images of U2OS cells expressing an empty vector (pLenti) or MISO-Flag. Yellow arrows indicate MEMS. Scale bars: 500 nm.

b-c. Representative images (b) and corresponding quantification (c) of U2OS cells expressing an empty vector (pLenti) or MISO-Flag, incubated with nonyl acridine orange (NAO). Scale bars: main panels 10 µm, magnified insets 5 µm.

d. Representative images showing the absence of ATP5a and MIC60 within MEMS. Scale bars: 1 µm

e. Representative fluorescence and electron microscopy images of U2OS cells expressing APEX2-MISO or MISO-APEX2. Scale bars: main panels 10 µm, magnified insets 2 µm for fluorescence images; 500 nm for TEM images.

f. A Model illustrating the topology of MISO within the inner mitochondrial membrane (IMM).

g. Quantification of mitochondrial morphology from (e).

h. Crosslinking analysis of MISO oligomerization by disuccinimidyl glutarate (DSG) in U2OS cells expressing MISO-Flag.

i. Co-immunoprecipitation with anti-Flag to validate the self-interaction of MISO.

j. Scheme of constructions of engineered MISO. MISO was segmented into N (1-59 AAs) and C (60-294 AAs) structural domain. The N terminus was replaced by a peptide localized to the outer mitochondrial membrane (TOMM20, 1-33 AAs) or inner mitochondrial membrane (BCS1, 1-49 AAs), which were fused to C regions.

k. Model illustrating the dynamics of mitochondrial morphology by OMM-MISO or IMM-MISO.

I-m. Representative images (l) and corresponding quantification (m) of mitochondrial morphology in U2OS cells expressing OMM-GFP or OMM-MISO. Scale bars: main panels 10 μm, magnified insets 5 μm.

n-o. Representative images (n) and corresponding quantification (o) of mitochondrial morphology in U2OS cells expressing IMM-GFP or IMM-MISO. Scale bars: main panels 10 μm, magnified insets 5 μm.

All data are presented as mean ± SD. c, g, m, o: two-tailed unpaired t test.